Journal of Controlled Release 158 (2012) 346–353

Contents lists available at SciVerse ScienceDirect

Journal of Controlled Release

journal homepage: www.elsevier.com/locate/jconrel

Nanobody-coupled microbubbles as novel molecular tracer

Sophie Hernot [a,*], Sunil Unnikrishnan [b], Zhongmin Du [b], Talent Shevchenko [b], Bernard Cosyns [a,c], Alexis Broisat [d], Jakub Toczek [d], Vicky Caveliers [a,e], Serge Muyldermans [f,g], Tony Lahoutte [a,e], Alexander L. Klibanov [b], Nick Devoogdt [a]

[a] In vivo Cellular and Molecular Imaging, Vrije Universiteit Brussel, Laarbeeklaan 103, 1090 Brussels, Belgium
[b] Cardiovascular Division MR4 Rm3147, University of Virginia School of Medicine, 409 Lane Road, Charlottesville, 22908 VA, USA
[c] Department of Cardiology, UZBrussel, Laarbeeklaan 101, 1090 Brussels, Belgium
[d] Radiopharmaceutiques Biocliniques, INSERM, U1039, Faculté de Médecine de Grenoble, Domaine de la Merci, Bat. Jean Roget, 38700 La Tronche, France
[e] Department of Nuclear Medicine, UZBrussel, Laarbeeklaan 101, 1090 Brussels, Belgium
[f] Laboratory of Cellular and Molecular Immunology, Vrije Universiteit Brussel, Pleinlaan 2, 1050 Brussels, Belgium
[g] Department of Structural Biology, Vlaams Instituut voor Biotechnologie, Pleinlaan 2, 1050 Brussels, Belgium

ARTICLE INFO

Article history:
Received 28 August 2011
Accepted 7 December 2011
Available online 16 December 2011

Keywords:
Targeted microbubbles
Contrast-enhanced ultrasound
Nanobodies
VCAM-1
Metabolic biotinylation

ABSTRACT

Camelid-derived single-domain antibody-fragments (~15 kDa), called nanobodies, are a new class of molecular tracers that are routinely identified with nanomolar affinity for their target and that are easily tailored for molecular imaging and drug delivery applications. We hypothesized that they are well-suited for the design of targeted microbubbles (μBs) and aimed to develop and characterize eGFP- and VCAM-1-targeted μBs. Anti-eGFP (cAbGFP4) and anti-VCAM-1 (cAbVCAM1-5) nanobodies were site-specifically biotinylated in bacteria. This metabolic biotinylation method yielded functional nanobodies with one biotin located at a distant site of the antigen-binding region of the molecule. The biotinylated nanobodies were coupled to biotinylated lipid μBs via streptavidin–biotin bridging. The ability of μB-cAbGFP4 to recognize eGFP was tested as proof-of-principle by fluorescent microscopy and confirmed the specific binding of eGFP to μB-cAbGFP4. Dynamic flow chamber studies demonstrated the ability of μB-cAbVCAM1-5 to bind VCAM-1 in fast flow (up to 5 dynes/cm^2). *In vivo* targeting studies were performed in MC38 tumor-bearing mice ($n=4$). μB-cAbVCAM1-5 or control μB-cAbGFP4 were injected intravenously and imaged using a contrast-specific ultrasound imaging mode. The echo intensity in the tumor was measured 10 min post-injection. μB-cAbVCAM1-5 showed an enhanced signal compared to control μBs ($p<0.05$). Using metabolic and site-specific biotinylation of nanobodies, a method to develop nanobody-coupled μBs was described. The application of VCAM-1-targeted μBs as novel molecular ultrasound contrast agent was demonstrated both *in vitro* and *in vivo*.

1. Introduction

Ultrasound contrast agents or microbubbles (μBs) are micron-sized particles filled with gas that strongly scatter ultrasound. They are widely used for organ edge delineation and perfusion imaging [1,2]. By targeting them, μBs can adhere selectively to cellular epitopes and receptors within the vasculature. Hence, contrast-enhanced ultrasound has been applied in experimental animal settings to depict molecular events such as inflammation [3,4], angiogenesis [5,6], thrombi [7,8], etc. Furthermore, since μBs have also been proposed as drug delivery systems, μB and drug accumulation in diseased tissues could be improved by selective targeting [9].

Active targeting requires ligands (antibodies or peptides) on the surface of the μB. Given the extremely high affinity and stable interaction between biotin and streptavidin, and the wide availability of biotinylated ligands, streptavidin–biotin linkage is a commonly used technique for coupling ligands to the μB's surface [6, 10-14]. The biotinylation of a ligand is usually performed chemically. However, this is a random process that might affect the binding capacity of the ligand. In metabolic biotinylation, the protein of interest is genetically fused to a biotin acceptor domain, where biotin protein ligases then post-translationally catalyze the covalent binding of biotin, resulting in site-specific biotinylation of the protein [15]. In the present study we used nanobodies as ligands for μB targeting. Nanobodies are small (~15 kDa) antigen-binding fragments derived from *camelid* heavy-chain antibodies [16,17]. Besides their high affinity, stability, solubility and yield [18], their monomeric behavior and carboxy-terminus that is located on the opposite side of the paratope, makes

* Corresponding author. Tel.: +32 2 477 49 91.
E-mail addresses: Sophie.Hernot@gmail.com (S. Hernot), su5z@virginia.edu (S. Unnikrishnan), ZD3Y@hscmail.mcc.virginia.ed (Z. Du), tshevchenkoi@gmail.com (T. Shevchenko), bcosyns@gmail.com (B. Cosyns), Alexis.Broisat@inserm.fr (A. Broisat), jakub.toczek@gmail.com (J. Toczek), vicky.caveliers@uzbrussel.be (V. Caveliers), svmuylde@vub.ac.be (S. Muyldermans), lahoutte@gmail.com (T. Lahoutte), sasha@virginia.edu (A.L. Klibanov), ndevoogd@vub.ac.be (N. Devoogdt).

0168-3659/$ – see front matter © 2011 Elsevier B.V. All rights reserved.
doi:10.1016/j.jconrel.2011.12.007

them ideal candidates to tailor into all kinds of formats: fusion of protein tags [18,19], bivalent or bispecific constructs [20,21], enzyme or toxin conjugates [22,23] and nanobody-GFP fused chromobodies [24]. Nanobodies have already been generated against a multitude of antigens, including the enhanced Green Fluorescent Protein (eGFP) [24]. Moreover, our group recently generated and selected a lead nanobody, named cAbVCAM1-5 with specific binding activity against the inflammation marker Vascular Cell Adhesion Molecule-1 (VCAM-1), and which is cross-reactive for both the murine and human VCAM-1. We demonstrated its preclinical application for the detection of atherosclerotic plaques with SPECT/CT [25]. In the present study, we describe the metabolic biotinylation of two nanobodies to develop targeted μBs. eGFP-targeted μBs are generated as a proof-of-principle. The VCAM-1-targeted μBs are characterized and subsequently tested for functionality, both *in vitro* in a flow chamber setting and *in vivo* in a murine subcutaneous tumor model.

2. Materials and methods

2.1. Cell lines

The mouse cell line bEND5 was purchased from the ATCC collection (Manassas, VA, USA). The murine adenocarcinoma cell line MC38 was a generous gift from J. Schlom, NIH. Both cell lines were grown in complete DMEM medium (Gibco BRL, Grand Island, NY, USA) and kept in culture in a humidified incubator at 37 °C and 5% CO_2. VCAM-1 expression on bEND5 cells was upregulated upon TNF-α stimulation (10 ng/mL) (Duchefa Biochemie, Haarlem, The Netherlands) for 18 h [26,27].

2.2. Expression and purification of biotinylated nanobodies

The genes encoding the nanobodies cAbGFP4 [24] and cAbVCAM1-5 [25] were recloned using the restriction enzymes NcoI and BstEII into the pBAD17 plasmid vector containing a Biotin Acceptor Domain (ASGGLNDIFEAQKIEWHGSSKYKY) preceded by an IgA hinge (SPSTPPTPSPSTPP), downstream of the nanobody sequence [28]. Each of these plasmid constructs was co-transformed in *Escherichia coli* WK6 cells together with the BirA plasmid (encoding for a Biotin-Protein Ligase) (AviTag, Avidity LLC, Aurora, CO, USA). Bacteria were grown at 37 °C in flasks filled with 330 ml Terrific Broth medium supplemented with 0.1% glucose, D-Biotin (50 μM) (Acros Organics, Morris Plains, NJ, USA) and under selection of both ampicillin (100 μg/ml) and chloramphenicol (35 μg/ml) (Sigma-Aldrich, Steinheim, Germany) until the exponential growth phase was reached. Nanobody expression was induced by adding isopropyl β-D-1-thiogalactopyranoside (Duchefa Biochemie) to 1 mM and incubating the cultures at 28 °C overnight. Nanobodies were extracted from the periplasm of pelleted bacteria by osmotic shock as described previously [18] and the free D-biotin was eliminated by dialysis. Biotinylated nanobodies were further purified on a Streptavidin–Mutein Matrix (Roche, Vilvoorde, Belgium) and eluted by competition with 2 mM D-biotin according to the manufacturer's protocol. The eluates were finally subjected to size-exclusion chromatography on a Superdex HR75 10/300 column with PBS as elution buffer at a flow rate of 0.5 ml/min.

2.3. Characterization of biotinylated nanobodies

The purity of the biotinylated nanobodies was assessed by Coomassie Blue-stained SDS-PAGE. To verify the biotinylation of the nanobodies, a Western Blot was performed with Extravidin-AP (Sigma-Aldrich) detection and development with NBT/BCIP.

For flow cytometry, 1×10^6 TNF-α stimulated bEND5 and non-stimulated bEND5 cells (negative control) were incubated with 1 μg biotinylated cAbVCAM1-5 or cAbGFP4 for 1 h at 4 °C and binding was detected with 500 ng streptavidin-PE (Sigma-Aldrich) on a FACS Canto II analyzer (BD Biosciences, Franklin Lakes, NJ, USA). Data were analyzed with FlowJo software (TreeStar, Ashland, OR, USA).

Surface Plasmon Resonance was used, as previously described [25] using a T100 instrument (Biacore, GE Healthcare), to determine the affinity parameter K_D (dissociation constant) of the biotinylated cAbVCAM1-5 for mouse VCAM-1/Fc-His (R&D Systems Inc., Minneapolis, MN, USA) and enable comparison with the non-biotinylated, original cAbVCAM1-5 nanobody.

2.4. Preparation of targeted microbubbles

Biotinylated μBs were prepared as described earlier [29]. First, a lipid micellar aqueous dispersion was prepared by sonication of the saline-lipid mixture containing 2 mg/ml phosphatidylcholine (Avanti Lipids, Alabaster, AL, USA), 2 mg/ml PEG-stearate (Sigma Aldrich, St. Louis, MO, USA) and 0.1 mg/ml biotin-PEG3400-phosphatidylethanolamine (Shearwater, Birmingham, AL, USA). Then decafluorobutane gas (F2 Chemicals Ltd, Lea Town, UK) was sparged through the aqueous phase and sonication continued at maximum power to generate μBs. For fluorescence tagging of μBs, trace amount (<1% of the mass of other lipids) of the lipid dye DiI (Molecular Probes, Eugene, OR, USA) was added to the lipid mixture.

Biotinylated nanobodies were conjugated to the surface of the μBs by biotin-streptavidin bridging chemistry. 3 μg of streptavidin (Anaspec Inc., Fremont, CA, USA) was added per 10^7 μBs and incubated for 15 min, followed by three washing steps by centrifugational floatation. Subsequently, 1 μg biotinylated nanobody was incubated per 10^7 μBs for 1 h at 4 °C and washed again. Particle concentration, surface area and size-distribution of μBs were assessed using a Coulter counter (Coulter Multisizer 3, Beckman Coulter Inc., Brea, CA, USA).

As proof of principle, 300×10^6 μB-cAbGFP4 or non-targeted μBs (biotinylated μBs without streptavidin and nanobodies) were incubated for 15 min with 1 μmol eGFP and washed 3 times. Bright field and fluorescent microscopy were used to detect binding of eGFP to the surface of the μBs.

2.5. Characterization of targeted μBs

To quantify the number of nanobodies coupled to the surface of the μBs, biotinylated cAbVCAM1-5 was first FITCylated using fluorescein isothiocyanate (FITC) (Sigma Aldrich) to a ratio of 1.3 FITC molecules per nanobody, and purified by centrifugal filtration. Biotinylated cAbVCAM1-5-FITC was then coupled to non-fluorescent μBs in the same conditions as described above. The amount of FITC-nanobody fluorescence on the μBs was measured with a spectrofluorometer (SpectraMAX Gemini XS, Molecular Devices Inc., Sunnyvale, CA, USA) after μB destruction by pressurization. A FITC standard was used to convert the fluorescent signal to the number of FITC molecules, and thus to the number of nanobodies. The experiment was performed in triplicate.

Maximal nanobody occupancy of the μB's surface was ascertained by adding different amounts of cAbGFP4 (0, 0.01, 0.1, 1 and 10 times the standard amount described above, which is 1 μg biotinylated nanobody per 10^7 microbubbles) to streptavidin-conjugated μBs, followed by a saturating amount of eGFP (1 μmol). The fluorescent signal on the different preparations was measured by flow cytometry and plotted against the amount of nanobody added.

2.6. In vitro dynamic binding studies: fluorescent and ultrasound imaging

Culture dishes (35 mm, Corning Inc, Corning, NY, USA) were coated with either 200 μl of 5 ng/μl recombinant mouse VCAM-1/Fc-His or only PBS overnight at 4 °C and blocked subsequently with 1% BSA (Sigma-Aldrich) in PBS. The dishes were mounted upside down in a parallel plate flow chamber system (Glycotech Inc., Gaithersburg, MD, USA) containing a silicon gasket 0.127 mm thick and a flow deck slit width of

2.5 mm. Targeted μBs were diluted in degassed perfluorocarbon-saturated PBS containing 1% BSA and were drawn through the flow chamber using a syringe pump (Harvard Apparatus Inc., Holliston, MA, USA). The flow rate was adjusted to obtain the desired wall shear stress (WSS) based on following formula:

$$\tau_w = 6\mu Q/_{a^2 b}$$

where τ_w = wall shear stress (dynes/cm^2), μ = apparent viscosity (1 cP = 0.01 dynes s/cm^2), a = channel height (0.0127 cm), b = channel width (0.25 cm) and Q = volumetric flow rate (cm^3/s).

μB adherence to VCAM-1 was detected by two different methods: fluorescent microscopy and contrast ultrasound imaging. For the first method, a field of view of 140 μm × 105 μm in the middle of the flow chamber was imaged with an upright fluorescent microscope (40× water immersion objective) focused at the reactive surface of the flow chamber. μBs were suspended at a concentration of 5×10^6/ml. The flow of fluorescent μB-cAbVCAM1-5 at 0.5, 1.0, 1.5 and 2.0 dynes/cm^2 was monitored by video microscopy for 5 min after equilibration with a standard NTSC camera. The number of adherent and free-flowing near-wall μBs was counted manually ($n \geq 3$ for control blank dishes, $n \geq 10$ for VCAM-1-coated dishes). The binding efficiency was calculated as the fraction of the near-wall flowing bubbles that adhered to the surface.

For the second method using ultrasound, the flow chamber was submersed in a water bath. An ultrasound transducer (15L8-S, Siemens, Acuson Sequoia 512) was positioned in such way that a longitudinal section of the flow chamber was visualized within the imaging plane ($n \geq 4$ for each condition). Specular reflection from the flow chamber assembly was kept to a minimum by choosing the positioning angles. To measure the acoustic reflection generated by the μBs, the US settings were set as follows: Cadence CPS mode, frequency 7 MHz, mechanical index (MI) of 0.18. μB-cAbVCAM1-5 were suspended at a concentration of 2.5×10^6/ml and allowed to flow through the chamber for 5 min at WSS of 1.0, 1.5, 2.0, 3.0 and 5.0 dynes/cm^2 (Step 1). Unbound μBs were then washed away with 1% BSA for another 5 min (Step 2) at 2.0 dynes/cm^2 if WSS in step 1 was ≤ 2.0 dynes/cm^2 or with a WSS equal to the WSS in step 1. The background signal was measured after destroying the adherent μBs at the end of step 2 by increasing the MI to 1.9 for 10 s (Step 3). Specificity of the binding of μB-cAbVCAM1-5 to the VCAM-1 antigen for WSS 1.5 dynes/cm^2 was confirmed by the antibody-blocking study. The coated dish was preincubated for 10 min with 5 μM non-biotinylated cAbVCAM1-5 and 5 μM of the same was added to the μB solution. Images were recorded and video clips of 3 s each at a frame rate of 10 Hz were imported into ImageJ software (NIH, Bethesda, MD, USA). Based on the images from step 1, a ROI (region of interest) was drawn around the flow chamber, and copied to the images of step 2 and 3. The mean pixel intensity in the ROIs in step 2 and step 3 was calculated and background signal (step 3) was subtracted from the images of step 2.

2.7. Immunohistochemistry

MC38 tumors were embedded in paraffin and 5 μm-thick sections were prepared. Following blocking with 10% horse serum in PBS and avidin blocking reagent (sp-2001, Vector Laboratories, Burlingame, CA, USA), adjacent sections were incubated overnight at 4 °C with the primary antibodies anti-VCAM-1 (10 ng/mL, sc-1504, Santa Cruz Biotechnology, Santa Cruz, CA, USA) and anti-PECAM-1 (endothelium staining, 10 ng/mL, sc-1506, Santa Cruz Biotechnology). The biotin-conjugated secondary horse-anti-goat IgG (BA-9500, Vector Laboratories) was incubated for 1 h at room temperature, followed by addition of the ABC reagent (PK7100, Vector Laboratories) for 45 min at room temperature. Finally, DAB solution (Sigma Aldrich) was used as chromogen reagent. Positive reaction was shown as a brown color. Sections were counterstained with hematoxylin.

2.8. Tumor model and in vivo contrast-enhanced imaging

Animal protocols were approved by the Institutional Animal Care and Use Committee (IACUC) office at the University of Virginia. 0.5×10^6 MC38 tumor cells were injected subcutaneously in the hindlimb of female C57Bl/6 mice (>26 weeks old, $n = 4$) (NCI, Frederick, MD, USA). Tumors were allowed to grow for 12 days.

Mice were anesthetized with 2% isoflurane, placed on a warm pad and the 15L8-S ultrasound probe was positioned to image the cross-section of the tumor. A B-mode image of the tumor was first obtained, which was used to serve as an anatomical reference for quantification. Two bolus intravenous injections of 37.5×10^6 μBs (μB-cAbVCAM1-5 or the control μB-cAbGFP4, in random order) were performed 30 min apart and with the mouse and ultrasound probe in the same position. μB accumulation and clearance from the tumor vasculature was imaged over 10 min using the non-destructive contrast-specific Cadence CPS imaging mode (7 MHz, MI 0.20). After 10 min, the remaining μBs were destroyed with two high intensity ultrasound pulses 1 s apart (frequency 7 MHz, MI 1.9).

Image analysis was performed using Image J. A ROI was drawn on the digitized B-mode image to delineate the tumor. This ROI was copied to the contrast-specific images and mean pixel intensity in the ROI's was measured (as an average of 40 frames over 4 s). Once the tumor was completely perfused (~20 s after injection), maximal mean pixel intensity was obtained. Background signal (due to tissue signal and residual circulating contrast after 10 min) was measured immediately after high-intensity destruction of the μBs. Contrast enhancement from μB adherence at 10 min after reaching maximal peak intensity was determined just prior to μB destruction, corrected for background and expressed as percentage of the maximal mean pixel intensity.

2.9. Statistical analysis

Data were expressed as mean ± standard deviation. Results from *in vitro* binding studies were analyzed using the unpaired Student *t*-test and Dunnett's *t*-test. For the analysis of *in vivo* imaging data, a paired Student *t*-test was used. All statistical analyses were performed using SPSS Statistics 19 (IBM). *p*-Values < 0.05 were considered significant.

3. Results

3.1. Expression, purification and characterization of biotinylated nanobodies

The biotinylated nanobodies cAbGFP4 and cAbVCAM1-5 were produced at a final yield of 0.26 mg/L and 0.21 mg/L bacterial culture, respectively. Both were extracted from the periplasm, purified by affinity chromatography and eluted after size-exclusion chromatography as single symmetrical peaks. SDS-PAGE and Western Blot confirmed the purity and biotinylation of the nanobodies with the expected molecular weight (Fig. 1A and B).

As shown in Fig. 1C, biotinylated cAbVCAM1-5 was able to recognize VCAM-1 expressed on TNF-α stimulated cells, while this nanobody does not bind to VCAM-1-negative, non-stimulated cells. No binding to either stimulated or non-stimulated cells was detected for the biotinylated cAbGFP4 nanobody.

The K_D of biotinylated cAbVCAM1-5 for mouse VCAM-1 as measured by Surface Plasmon Resonance was 7.2 nM. As determined in this study, comparable sensograms and K_D-value (10.7 nM) were obtained for the original non-biotinylated format [25]. The sensograms are included as supplemental material.

3.2. Characterization of targeted microbubbles

Biotinylated nanobodies were attached to the surface of biotinylated μBs via a streptavidin linker. The antigen-binding loops of the

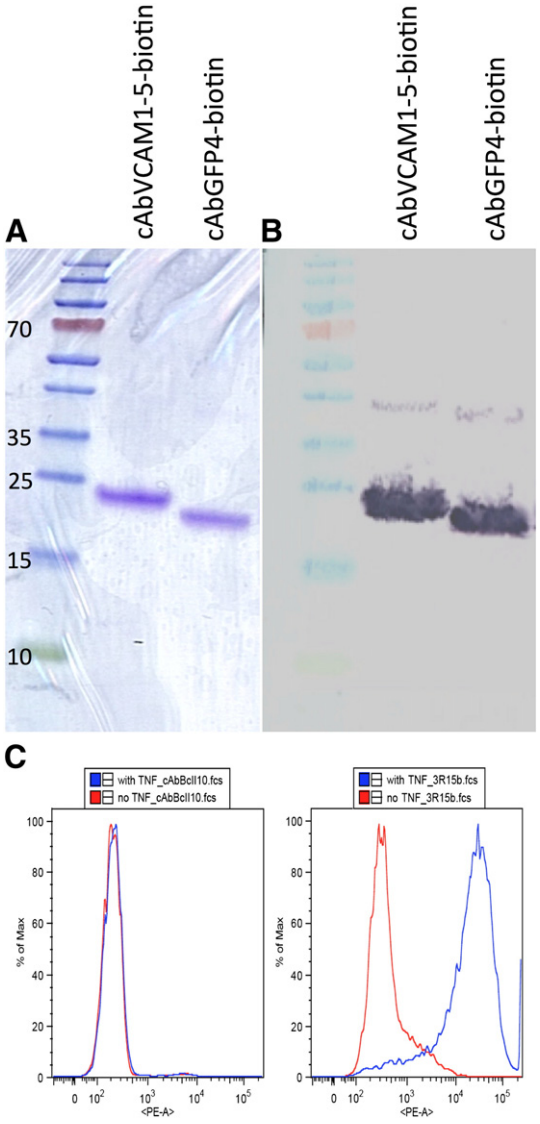

Fig. 1. SDS-PAGE (A) and Western Blot (B) of the purified biotinylated nanobodies cAbVCAM1-5 and cAbGFP4. (C) Flow cytometric analysis of cAbVCAM1-5 and control (cAbGFP4) nanobody on non-treated (red) or TNFα-treated (blue) mouse bEND5 cells.

nanobodies should be oriented away from the μB as the biotin is located within a peptide stretch at the C-terminal end of the nanobody and separated by a protease resistant flexible IgA-linker. Hence the paratope of the nanobody on the μB should be well accessible to target its cognate antigen.

Addition of eGFP to a solution containing μB-cAbGFP4 resulted in the binding of eGFP to the surface of these targeted μBs as observed by fluorescence microscopy (Fig. 2A). Non-targeted μBs were not recognized by the eGFP and thus did not appear fluorescent.

Targeted μBs had a mean number-based diameter of 2.2 ± 0.2 μm, with a polydispersity index of 1.32. The coupling of streptavidin and biotinylated nanobodies did not influence their size-distribution (data not shown). The average number of biotinylated nanobodies coupled to the surface of a μB was calculated to be $288\,000 \pm 38\,000$, corresponding to one nanobody molecule every ~95 nm^2 or ~10^4 nanobodies per μm^2 of the μB surface. As demonstrated in the flow cytometric analysis in Fig. 2B, saturation of the μB's surface with nanobodies was achieved with the preparation conditions described above.

3.3. In vitro dynamic binding studies: fluorescent and ultrasound imaging

The results of the dynamic binding studies with fluorescence and ultrasound detection are shown in Figs. 3 and 4, respectively. Using both techniques, a significantly higher binding of μB-cAbVCAM1-5 was observed to dishes coated with the VCAM-1 antigen than for the non-coated ones. This was the case for all applied WSS ($p<0.05$). However, binding decreased with increasing WSS. With video microscopy, no μB binding to the target dish was observed at WSS > 2.0 dynes/cm^2 (data not shown), but significant binding of targeted μBs to its antigen could be detected up to 5 dynes/cm^2 using ultrasound imaging. Binding of μB-cAbVCAM1-5 to immobilized VCAM-1 protein is specific since blocking the antigen with an excess of non-biotinylated cAbVCAM1-5 significantly reduced adherence of the targeted μBs ($p<0.05$) (Fig. 4C).

3.4. In vivo contrast-enhanced imaging and immunohistochemistry

As an *in vivo* model for endothelium-expressed VCAM-1, we used the MC38 subcutaneous murine tumor model. Immunohistochemistry demonstrated expression of VCAM-1 (Fig. 5A) in the tumor vasculature (Fig. 5B). Non-specific staining of the secondary antibody was not observed (not shown).

Following injection of μBs, contrast-enhancement peaked rapidly (~ 20 s post-injection), after which the signal decreased (Fig. 6A). Ten minutes after μB-cAbVCAM1-5 intravenous injection, ultrasound contrast signal was observed to persist within the tumor. This signal was significantly higher compared to the signal of control μB-cAbGFP4 (Fig. 6B, C). After the bursting of the μBs, the signal almost completely disappeared, indicating that the majority of unbound circulating μBs had cleared from the bloodstream.

4. Discussion

Ultrasound imaging is increasingly making use of targeted μBs to evaluate intravascular molecular events emerging during disease progression [30-32]. In the animal model setting, this has become an established technique. In this study, μB targeting was performed using a new type of molecular probe, more precisely site-specifically biotinylated nanobodies. We first characterized μB targeting *in vitro* in a flow chamber and subsequently demonstrated that they could target intravascular VCAM-1 in an *in vivo* model of inflamed tumor vasculature.

The so-called protein tags are specific peptide sequences genetically grafted onto a recombinant protein. There are now numerous types of tags available suited to diverse applications and several have been fused successfully to nanobodies for affinity purification [18], epitope detection, protein localization [24], and radiolabeling [33,34]. In this study we introduced a biotin ligase tag at the carboxyterminal end of the nanobody and cotransfected a plasmid coding for the *E. coli* biotin ligase protein BirA, whose role consists of attaching the exogenously added biotin to this tag [15]. Using this enzymatic biotinylation technique, we obtain exactly one biotin per nanobody molecule positioned at the location of the tag. This is in contrast to chemical biotinylation where functional groups like lysines are required, resulting in different degrees of biotinylation, spread all over the protein. Moreover, the position of the biotin at the nanobody's carboxyterminal end is favorable for the orientation of the nanobody on the μB's surface. As the biotin-tag is located far away of the antigen binding loops involved in antigen recognition, the risk of compromising the binding capacity of the nanobody is minimized. Indeed, we demonstrated with flow cytometry as well as with affinity measurement experiments that the functionality and affinity of VCAM-1-specific nanobody was not altered by biotinylation. The cAbVCAM1-5 nanobody retained its affinity in the low nanomolar range [25]. In addition, the biotin tag provides a means of purifying the biotinylated nanobody on a streptavidin–mutein matrix [35,36], and isolating it from the possible untagged protein. The production

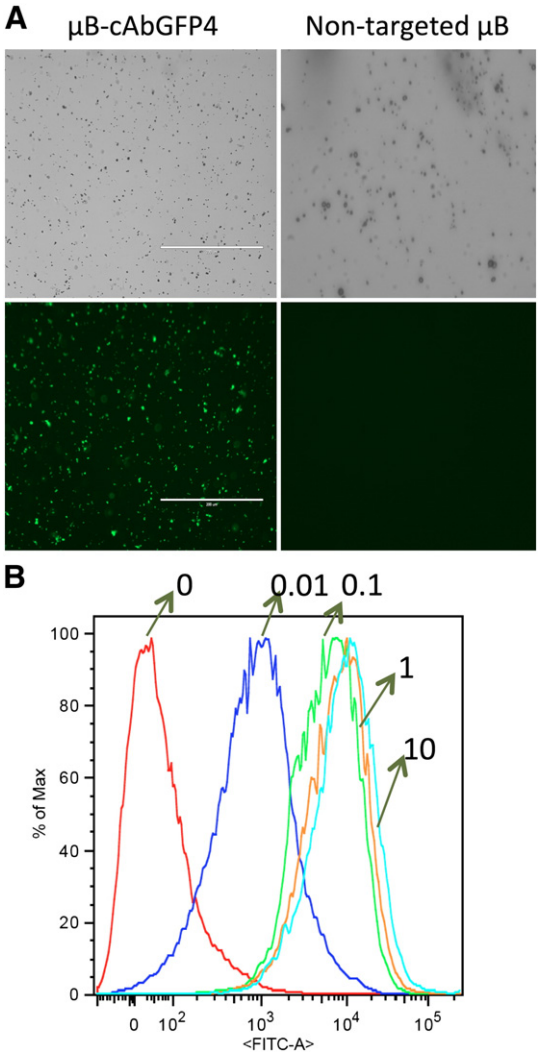

Fig. 2. (A) Bright field (BF) and fluorescent microscopy images showing binding of eGFP to μB-cAbGFP4 and not to non-targeted μBs. (Scale bar: 200 μm, 20× magnification) (B) Flow cytometric analysis of μBs bearing increasing amounts of cAbGFP4 on their surface (0, 0.01, 0.1, 1 and 10 times the standard added amount, which is 1 μg biotinylated nanobody per 10^7 microbubbles).

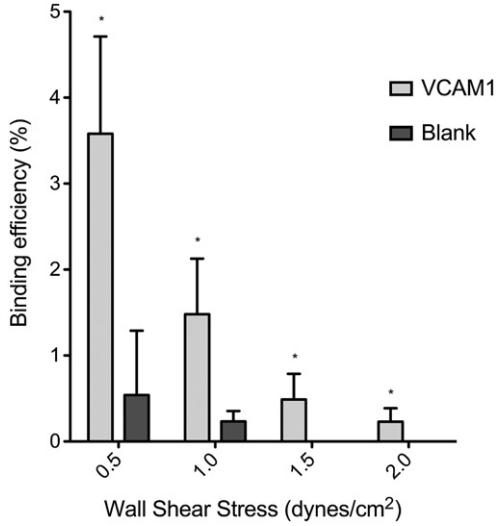

Fig. 3. μB-cAbVCAM1-5 binding efficiency (%) determined by fluorescence microscopy in a parallel plate flow chamber coated with VCAM-1 or no antigen (blank) as a function of the wall shear stress. $^*p<0.01$ for μB adherence on VCAM-1 coated flow chambers compared to non-coated flow chambers at same WSS.

yield of the biotinylated anti-eGFP and anti-VCAM-1 nanobodies (both ±0.25 mg/L) was significantly lower compared to that of the original formats (respectively 3 and 10 mg/L [25]). As nanobodies are transported to the periplasm, while BirA in this study remains within the cytoplasm, the biotinylation yield could be possibly increased by redirecting BirA to the periplasmic compartment where the nanobody is targeted as well [37].

Coupling of nanobodies to the μB's surface was achieved using the standard biotin-streptavidin bridging system. This is a common procedure because it is rapid, efficient and biotinylated ligands and antibodies are widely available. Using a direct measurement method with fluorescently labeled nanobodies, the nanobody surface coverage was estimated at approximately 3×10^5 per bubble and we demonstrated that maximal coverage was reached. This number is consistent with the results from previous studies using the same or other types of μBs. In those studies, monoclonal antibodies, Fab fragments or carbohydrate polymers [12,13,38-40] were bound to the μB's surface with values ranging from 3×10^4 to 3×10^5 molecules per μB. Bivalent and even bispecific nanobodies are easily generated and could be used to design dual-targeted μBs [20,21].

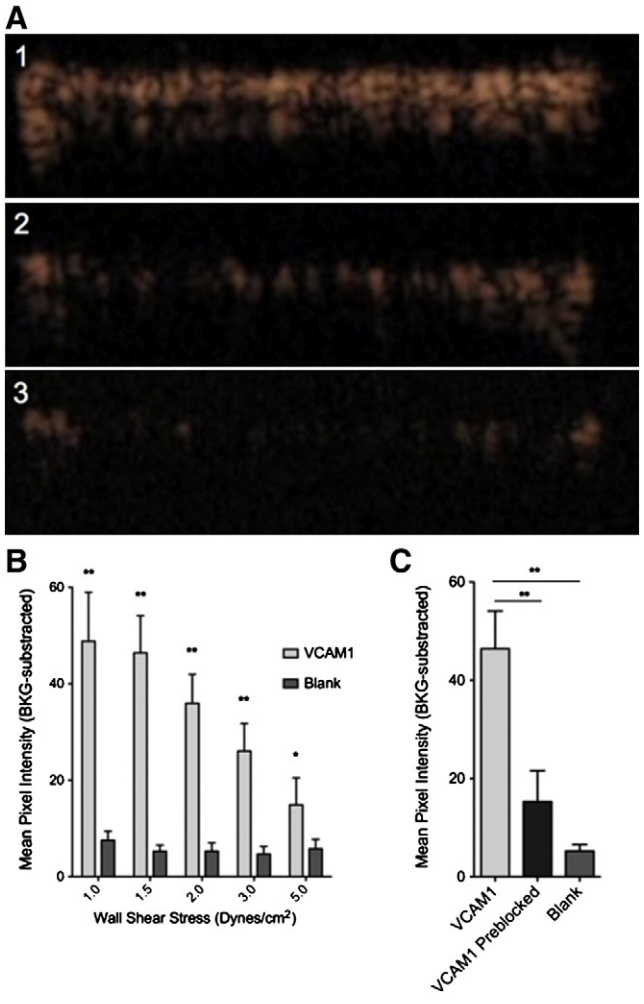

Fig. 4. (A) Representative images and (C) quantification of mean pixel intensity in flow chamber coated with VCAM-1 (A1), with pre-blocked VCAM-1 (A2) or without VCAM-1 (A3) after infusion of μB-cAbVCAM1-5 at 1.5 dynes/cm^2 and washing, as observed by contrast-specific ultrasound imaging. (B) Quantification of mean pixel intensity in flow chamber coated with or without VCAM-1 for different WSS. $^{**}p<0.001$ and $^*p<0.05$ for μB adherence on VCAM-1 coated flow chambers compared to non-coated flow chambers or pre-blocked VCAM-1 coated chambers at same WSS.

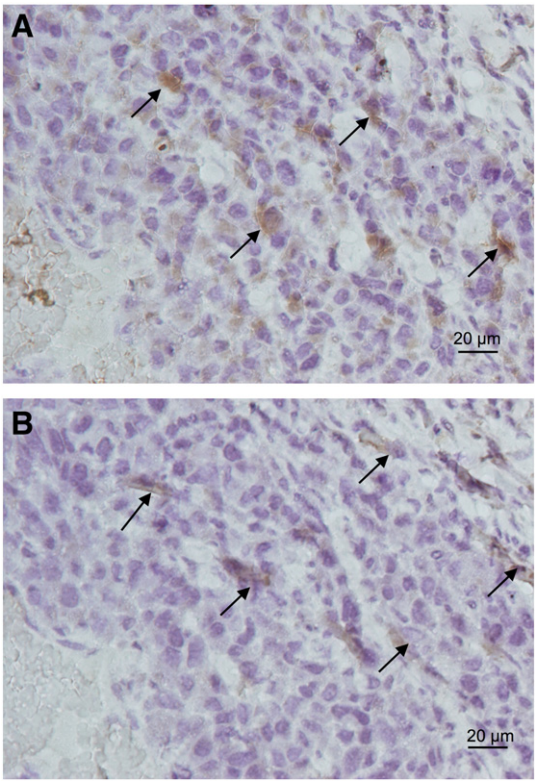

Fig. 5. Immunohistochemical analysis of adjacent MC38 xenograft tumor sections: (A) VCAM-1-specific and (B) PECAM-1 specific staining (endothelium). Intratumoral VCAM-1 expression (in brown) is observed in the tumor vasculature (black arrows) as well as on cancer cells.

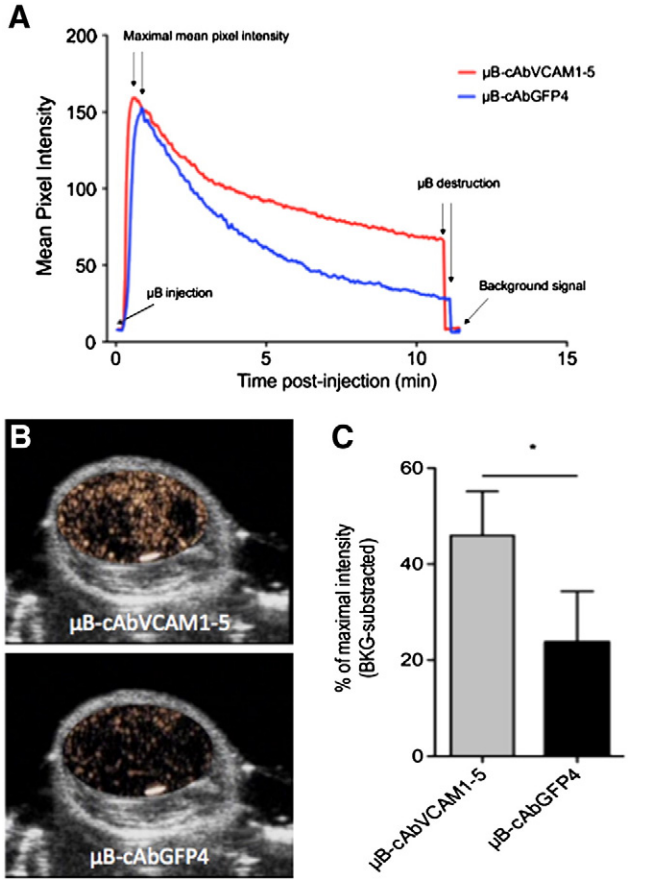

Fig. 6. (A) Representative time-course curves of contrast-enhancement in tumor following injection of μB-cAbVCAM1-5 and μB-cAbGFP4 (control). (B) Transverse B-mode images of MC38 tumors overlaid with a ROI showing contrast-specific signal in tumor 10 min after intravenous injection of either μB-cAbVCAM1-5 (upper image) or μB-cAbGFP4 (lower image) in the same mouse. (C) Quantification of μB adherence in tumor, $^*p<0.05$ for comparison of contrast-specific signal in tumor after injection of μB-cAbVCAM1-5 and control μBs. Signal at 10 min post-injection was expressed as % of the maximal intensity reached ~ 20 s after injection, and corrected for background.

The functionality of the nanobody-conjugated μB system was first shown with eGFP-targeted μBs, as a proof-of-principle. In static flow conditions, eGFP rapidly and specifically recognized μB-cAbGFP4, making the μBs visible under fluorescence microscopy. For the VCAM-1-targeted μBs, binding to their antigen was studied under dynamic conditions in an antigen-coated flow chamber. The adherence of the μBs was detected both by fluorescence microscopy and ultrasound imaging. Both techniques gave comparable results. A significantly higher binding of the targeted μBs was observed in the presence of the antigen for the different WSS compared to the control non-coated chambers. However, as it is known, the flow rate has an important impact on the adherence of μBs and thus μB binding decreased with increasing WSS [38,40]. Targeting of μBs at higher WSS (up to at least 5 dynes/cm^2) could only be observed by ultrasound detection. Indeed, ultrasound has a much larger field of view as compared with microscopy (over three orders of magnitude), and ultrasound, like microscopy, can observe individual μBs [41]. Therefore, ultrasound allows the detection of μBs adherent to the target at much lower surface density. Additionally, ultrasonic detection of the μBs confirms that the targeted μBs are still acoustically responsive. In the literature, no adherence of μBs *in vitro* was reported above 6 dynes/cm^2, although dual targeted μBs and pulsatile flow have been shown to improve the binding efficiency at higher WSS [13]. While values in the range of the chosen WSS are found in tumor vasculature [42], microbubble targeting in larger vessels such as the abdominal aorta becomes more difficult [43]. There, other parameters such as turbulent flow, presence of blood components etc. might have additional influence on the μB targeting *in vivo*. Recently, it has been demonstrated that firm attachment of VCAM-1-targeted μBs could be achieved in combination with magnetic guidance [44].

The constitutive expression of the adhesion molecule VCAM-1 plays an important role in cell homing and cell trafficking [45,46], and its expression is induced by inflammatory cytokines on disturbed endothelium to mediate the recruitment of leukocytes [47-49]. The presence of VCAM-1 has been reported on cancer cells and/or on the tumor vasculature; however, it is tumor-dependent [50-53]. The exact role of VCAM-1 in tumors is still not known, but it seems to be involved in oncogenesis, angiogenesis, metastasis and immune response [54-56]. Targeting VCAM-1 expression in the tumor vasculature allows not only imaging of the inflammatory state of the tumor, but also the targeting of therapy [52]. As assessed by immunohistochemistry, expression of VCAM-1 was found on the MC38-tumor endothelium and this mouse tumor model was chosen to demonstrate the *in vivo* binding of the VCAM-1-targeted μBs. Indeed, 10 min after intravenous injection, the VCAM-1-targeted μBs showed a significantly higher adherence in the MC38 tumor's vasculature than the non-VCAM-1-targeted μBs, as was imaged with a contrast-specific ultrasound imaging mode. VCAM-1 is also known to be expressed in atherosclerotic plaques and contrast-enhanced ultrasound imaging of inflammation in such lesions was previously shown by Kaufmann *et al.* [3]. The application of anti-VCAM-1-nanobody-coupled μBs in such setting remains to be demonstrated.

Although nanobodies have comparable affinity parameters as monoclonal antibodies, other advantages of nanobodies over murine antibodies are their high stability (both chemical and thermal) [57]. In addition, their small size (~15 kDa) and the high degree of sequence identity (>80%) with the human VH sequences make them less likely to elicit immune responses in humans. Indeed, they are reported to have a

low immunogenicity [58]. Furthermore, humanization of nanobodies has been described previously [34,59]. The streptavidin–biotin coupling between nanobodies and μBs is not applicable in clinical setting because of the possible occurrence of immune reactions to streptavidin. Instead, other conjugation methods are preferred such as the covalent thiol–maleimide binding [60]. Geers et al. [61] applied this coupling reaction for the fabrication of self-assembly liposome-loaded μBs in a single step, which would ease the production of sterile material. The introduction of a cystein on the nanobody's carboxyterminal end (instead of the biotin acceptor tag), as demonstrated previously for attachment to gold particles [62], would thus be an elegant way to couple nanobodies site-specifically to maleimide-bearing μBs during or even before μB preparation. Such formulation of humanized nanobodies covalently attached to the μB shell in an oriented manner should be considered for preclinical development evaluation, and eventually may find its way into clinical practice.

5. Conclusion

Using a metabolic and site-specific biotinylation of nanobodies, nanobody-targeted μBs were prepared. We demonstrated the functionality of these nanobody-targeted μBs *in vitro* under a variety of flow conditions and this new molecular ultrasound contrast agent was subsequently used *in vivo* to detect VCAM-1 expression in the tumor vasculature.

Conflicts of interest statement

None.

Supplementary materials related to this article can be found online at doi:10.1016/j.jconrel.2011.12.007.

Acknowledgements

Tony Lahoutte is a Senior Clinical Investigator of the Research Foundation-Flanders (Belgium) (FWO). The research at ICMI is funded by the Interuniversity Attraction Poles Program, Belgian State, Belgian Science Policy and National Kankerplan Action 29. A.L. Klibanov acknowledges support via NIH R21/33 CA102880 for the studies performed at University of Virginia.

References

[1] J.R. Lindner, K. Wei, Contrast echocardiography, Curr. Probl. Cardiol. 27 (2002) 454–519.
[2] M. Postema, O.H. Gilja, Contrast-enhanced and targeted ultrasound, World J. Gastroenterol. 17 (2011) 28–41.
[3] B.A. Kaufmann, J.M. Sanders, C. Davis, A. Xie, P. Aldred, I.J. Sarembock, J.R. Lindner, Molecular imaging of inflammation in atherosclerosis with targeted ultrasound detection of vascular cell adhesion molecule-1, Circulation 116 (2007) 276–284.
[4] F.S. Villanueva, R.J. Jankowski, S. Klibanov, M.L. Pina, S.M. Alber, S.C. Watkins, G.H. Brandenburger, W.R. Wagner, Microbubbles targeted to intercellular adhesion molecule-1 bind to activated coronary artery endothelial cells, Circulation 98 (1998) 1–5.
[5] D.B. Ellegala, H. Leong-Poi, J.E. Carpenter, A.L. Klibanov, S. Kaul, M.E. Shaffrey, J. Sklenar, J.R. Lindner, Imaging tumor angiogenesis with contrast ultrasound and microbubbles targeted to alpha(v)beta3, Circulation 108 (2003) 336–341.
[6] J.K. Willmann, R. Paulmurugan, K. Chen, O. Gheysens, M. Rodriguez-Porcel, A.M. Lutz, I.Y. Chen, X. Chen, S.S. Gambhir, US imaging of tumor angiogenesis with microbubbles targeted to vascular endothelial growth factor receptor type 2 in mice, Radiology 246 (2008) 508–518.
[7] E.C. Unger, T.P. McCreery, R.H. Sweitzer, D. Shen, G. Wu, In vitro studies of a new thrombus-specific ultrasound contrast agent, Am. J. Cardiol. 81 (1998) 58G–61G.
[8] M. Takeuchi, K. Ogunyankin, N.G. Pandian, T.P. McCreery, R.H. Sweitzer, V.E. Caldwell, E.C. Unger, E. Avelar, M. Sheahan, R. Connolly, Enhanced visualization of intravascular and left atrial appendage thrombus with the use of a thrombus-targeting ultrasonographic contrast agent (MRX-408A1): in vivo experimental echocardiographic studies, J. Am. Soc. Echocardiogr. 12 (1999) 1015–1021.
[9] F. Yan, X. Li, Q. Jin, C. Jiang, Z. Zhang, T. Ling, B. Qiu, H. Zheng, Therapeutic ultrasonic microbubbles carrying paclitaxel and LyP-1 peptide: preparation, characterization and application to ultrasound-assisted chemotherapy in breast cancer cells, Ultrasound Med. Biol. 37 (2011) 768–779.
[10] A.L. Klibanov, Preparation of targeted microbubbles: ultrasound contrast agents for molecular imaging, Med. Biol. Eng. Comput. 47 (2009) 875–882.
[11] G.M. Lanza, K.D. Wallace, M.J. Scott, W.P. Cacheris, D.R. Abendschein, D.H. Christy, A.M. Sharkey, J.G. Miller, P.J. Gaffney, S.A. Wickline, A novel site-targeted ultrasonic contrast agent with broad biomedical application, Circulation 94 (1996) 3334–3340.
[12] G.E. Weller, F.S. Villanueva, A.L. Klibanov, W.R. Wagner, Modulating targeted adhesion of an ultrasound contrast agent to dysfunctional endothelium, Ann. Biomed. Eng. 30 (2002) 1012–1019.
[13] E.A. Ferrante, J.E. Pickard, J. Rychak, A. Klibanov, K. Ley, Dual targeting improves microbubble contrast agent adhesion to VCAM-1 and P-selectin under flow, J. Control. Release 140 (2009) 100–107.
[14] S. Pochon, I. Tardy, P. Bussat, T. Bettinger, J. Brochot, M. von Wronski, L. Passantino, M. Schneider, BR55: a lipopeptide-based VEGFR2-targeted ultrasound contrast agent for molecular imaging of angiogenesis, Invest. Radiol. 45 (2010) 89–95.
[15] A. Chapman-Smith, J.E. Cronan Jr., In vivo enzymatic protein biotinylation, Biomol. Eng. 16 (1999) 119–125.
[16] C. Hamers-Casterman, T. Atarhouch, S. Muyldermans, G. Robinson, C. Hamers, E.B. Songa, N. Bendahman, R. Hamers, Naturally occurring antibodies devoid of light chains, Nature 363 (1993) 446–448.
[17] S. Muyldermans, Single domain camel antibodies: current status, J. Biotechnol. 74 (2001) 277–302.
[18] M. Arbabi Ghahroudi, A. Desmyter, L. Wyns, R. Hamers, S. Muyldermans, Selection and identification of single domain antibody fragments from camel heavy-chain antibodies, FEBS Lett. 414 (1997) 521–526.
[19] K.E. Conrath, M. Lauwereys, M. Galleni, A. Matagne, J.M. Frere, J. Kinne, L. Wyns, S. Muyldermans, Beta-lactamase inhibitors derived from single-domain antibody fragments elicited in the camelidae, Antimicrob. Agents Chemother. 45 (2001) 2807–2812.
[20] K. Els Conrath, M. Lauwereys, L. Wyns, S. Muyldermans, Camel single-domain antibodies as modular building units in bispecific and bivalent antibody constructs, J. Biol. Chem. 276 (2001) 7346–7350.
[21] I. Hmila, D. Saerens, R. Ben Abderrazek, C. Vincke, N. Abidi, Z. Benlasfar, J. Govaert, M. El Ayeb, B. Bouhaouala-Zahar, S. Muyldermans, A bispecific nanobody to provide full protection against lethal scorpion envenoming, FASEB J. 24 (2010) 3479–3489.
[22] V. Cortez-Retamozo, N. Backmann, P.D. Senter, U. Wernery, P. De Baetselier, S. Muyldermans, H. Revets, Efficient cancer therapy with a nanobody-based conjugate, Cancer Res. 64 (2004) 2853–2857.
[23] T.N. Baral, S. Magez, B. Stijlemans, K. Conrath, B. Vanhollebeke, E. Pays, S. Muyldermans, P. De Baetselier, Experimental therapy of African trypanosomiasis with a nanobody-conjugated human trypanolytic factor, Nat. Med. 12 (2006) 580–584.
[24] U. Rothbauer, K. Zolghadr, S. Tillib, D. Nowak, L. Schermelleh, A. Gahl, N. Backmann, K. Conrath, S. Muyldermans, M.C. Cardoso, H. Leonhardt, Targeting and tracing antigens in live cells with fluorescent nanobodies, Nat. Methods 3 (2006) 887–889.
[25] A. Broisat, S. Hernot, J. Toczek, J. De Vos, W. Werney, L. M. Riou, S. Martin, M. Ahmadi, N. Thielens, V. Caveliers, S. Muyldermans, T. Lahoutte, D. Fagret, C. Ghezzi, N. Devoogdt, Nanobodies Targeting Mouse/Human VCAM1 for Nuclear Imaging of Atherosclerotic Lesions, unpublished results.
[26] R.K. Rohnelt, G. Hoch, Y. Reiss, B. Engelhardt, Immunosurveillance modelled in vitro: naive and memory T cells spontaneously migrate across unstimulated microvascular endothelium, Int. Immunol. 9 (1997) 435–450.
[27] M. Laschinger, B. Engelhardt, Interaction of alpha4-integrin with VCAM-1 is involved in adhesion of encephalitogenic T cell blasts to brain endothelium but not in their transendothelial migration in vitro, J. Neuroimmunol. 102 (2000) 32–43.
[28] D. Saerens, F. Frederix, G. Reekmans, K. Conrath, K. Jans, L. Brys, L. Huang, E. Bosmans, G. Maes, G. Borghs, S. Muyldermans, Engineering camel single-domain antibodies and immobilization chemistry for human prostate-specific antigen sensing, Anal. Chem. 77 (2005) 7547–7555.
[29] A.L. Klibanov, J.J. Rychak, W.C. Yang, S. Alikhani, B. Li, S. Acton, J.R. Lindner, K. Ley, S. Kaul, Targeted ultrasound contrast agent for molecular imaging of inflammation in high-shear flow, Contrast Media Mol. Imaging 1 (2006) 259–266.
[30] A.L. Klibanov, M.S. Hughes, J.N. Marsh, C.S. Hall, J.G. Miller, J.H. Wible, G.H. Brandenburger, Targeting of ultrasound contrast material. An in vitro feasibility study, Acta Radiol. Suppl. 412 (1997) 113–120.
[31] B.A. Kaufmann, J.R. Lindner, Molecular imaging with targeted contrast ultrasound, Curr. Opin. Biotechnol. 18 (2007) 11–16.
[32] J.R. Lindner, Molecular imaging of myocardial and vascular disorders with ultrasound, JACC Cardiovasc. Imaging 3 (2010) 204–211.
[33] L.O. Gainkam, L. Huang, V. Caveliers, M. Keyaerts, S. Hernot, I. Vaneycken, C. Vanhove, H. Revets, P. De Baetselier, T. Lahoutte, Comparison of the biodistribution and tumor targeting of two 99mTc-labeled anti-EGFR nanobodies in mice, using pinhole SPECT/-micro-CT, J. Nucl. Med. 49 (2008) 788–795.
[34] I. Vaneycken, J. Govaert, C. Vincke, V. Caveliers, T. Lahoutte, P. De Baetselier, G. Raes, A. Bossuyt, S. Muyldermans, N. Devoogdt, In vitro analysis and in vivo tumor targeting of a humanized, grafted nanobody in mice using pinhole SPECT/-micro-CT, J. Nucl. Med. 51 (2010) 1099–1106.
[35] M.H. Qureshi, J.C. Yeung, S.C. Wu, S.L. Wong, Development and characterization of a series of soluble tetrameric and monomeric streptavidin muteins with differential biotin binding affinities, J. Biol. Chem. 276 (2001) 46422–46428.
[36] D. Juzumiene, C.Y. Chang, D. Fan, T. Hartney, J.D. Norris, D.P. McDonnell, Single-step purification of full-length human androgen receptor, Nucl. Recept. Signal. 3 (2005) e001.
[37] J.M. Niers, J.W. Chen, R. Weissleder, B.A. Tannous, Enhanced in vivo imaging of metabolically biotinylated cell surface reporters, Anal. Chem. 83 (2011) 994–999.

[38] A.M. Takalkar, A.L. Klibanov, J.J. Rychak, J.R. Lindner, K. Ley, Binding and detachment dynamics of microbubbles targeted to P-selectin under controlled shear flow, J. Control. Release 96 (2004) 473–482.
[39] A. Della Martina, E. Allemann, T. Bettinger, P. Bussat, A. Lassus, S. Pochon, M. Schneider, Grafting of abciximab to a microbubble-based ultrasound contrast agent for targeting to platelets expressing GP IIb/IIIa - characterization and in vitro testing, Eur. J. Pharm. Biopharm. 68 (2008) 555–564.
[40] G.E. Weller, F.S. Villanueva, E.M. Tom, W.R. Wagner, Targeted ultrasound contrast agents: in vitro assessment of endothelial dysfunction and multi-targeting to ICAM-1 and sialyl Lewisx, Biotechnol. Bioeng. 92 (2005) 780–788.
[41] A.L. Klibanov, P.T. Rasche, M.S. Hughes, J.K. Wojdyla, K.P. Galen, J.H. Wible Jr., G.H. Brandenburger, Detection of individual microbubbles of ultrasound contrast agents: imaging of free-floating and targeted bubbles, Invest. Radiol. 39 (2004) 187–195.
[42] W.S. Kamoun, S.S. Chae, D.A. Lacorre, J.A. Tyrrell, M. Mitre, M.A. Gillissen, D. Fukumura, R.K. Jain, L.L. Munn, Simultaneous measurement of RBC velocity, flux, hematocrit and shear rate in vascular networks, Nat. Methods 7 (2010) 655–660.
[43] L.M. Kornmann, K.D. Reesink, R.S. Reneman, A.P. Hoeks, Critical appraisal of targeted ultrasound contrast agents for molecular imaging in large arteries, Ultrasound Med. Biol. 36 (2010) 181–191.
[44] J. Wu, H. Leong-Poi, J. Bin, L. Yang, Y. Liao, Y. Liu, J. Cai, J. Xie, Efficacy of contrast-enhanced US and magnetic microbubbles targeted to vascular cell adhesion molecule-1 for molecular imaging of atherosclerosis, Radiology 260 (2011) 463–471.
[45] B.A. Schwarz, A. Bhandoola, Trafficking from the bone marrow to the thymus: a prerequisite for thymopoiesis, Immunol. Rev. 209 (2006) 47–57.
[46] M. Vermeulen, F. Le Pesteur, M.C. Gagnerault, J.Y. Mary, F. Sainteny, F. Lepault, Role of adhesion molecules in the homing and mobilization of murine hematopoietic stem and progenitor cells, Blood 92 (1998) 894–900.
[47] M.F. Iademarco, J.L. Barks, D.C. Dean, Regulation of vascular cell adhesion molecule-1 expression by IL-4 and TNF-alpha in cultured endothelial cells, J. Clin. Invest. 95 (1995) 264–271.
[48] E. Galkina, K. Ley, Vascular adhesion molecules in atherosclerosis, Arterioscler. Thromb. Vasc. Biol. 27 (2007) 2292–2301.
[49] J.D. van Buul, P.L. Hordijk, Endothelial signalling by Ig-like cell adhesion molecules, Transfus. Clin. Biol. 15 (2008) 3–6.
[50] A.J. Staal-van den Brekel, F.B. Thunnissen, W.A. Buurman, E.F. Wouters, Expression of E-selectin, intercellular adhesion molecule (ICAM)-1 and vascular cell adhesion molecule (VCAM)-1 in non-small-cell lung carcinoma, Virchows Arch. 428 (1996) 21–27.
[51] N. Jonjic, I. Martin-Padura, T. Pollicino, S. Bernasconi, P. Jilek, A. Bigotti, R. Mortarini, A. Anichini, G. Parmiani, F. Colotta, E. Dejana, A. Mantovani, P.G. Natali, Regulated expression of vascular cell adhesion molecule-1 in human malignant melanoma, Am. J. Pathol. 141 (1992) 1323–1330.
[52] A. Dienst, A. Grunow, M. Unruh, B. Rabausch, J.E. Nor, J.W. Fries, C. Gottstein, Specific occlusion of murine and human tumor vasculature by VCAM-1-targeted recombinant fusion proteins, J. Natl. Cancer Inst. 97 (2005) 733–747.
[53] I. Kuzu, R. Bicknell, C.D. Fletcher, K.C. Gatter, Expression of adhesion molecules on the endothelium of normal tissue vessels and vascular tumors, Lab. Invest. 69 (1993) 322–328.
[54] Y.B. Ding, G.Y. Chen, J.G. Xia, X.W. Zang, H.Y. Yang, L. Yang, Association of VCAM-1 overexpression with oncogenesis, tumor angiogenesis and metastasis of gastric carcinoma, World J. Gastroenterol. 9 (2003) 1409–1414.
[55] T.C. Wu, The role of vascular cell adhesion molecule-1 in tumor immune evasion, Cancer Res. 67 (2007) 6003–6006.
[56] C.A. Maurer, H. Friess, B. Kretschmann, S. Wildi, C. Muller, H. Graber, M. Schilling, M.W. Buchler, Over-expression of ICAM-1, VCAM-1 and ELAM-1 might influence tumor progression in colorectal cancer, Int. J. Cancer 79 (1998) 76–81.
[57] M. Dumoulin, K. Conrath, A. Van Meirhaeghe, F. Meersman, K. Heremans, L.G. Frenken, S. Muyldermans, L. Wyns, A. Matagne, Single-domain antibody fragments with high conformational stability, Protein Sci. 11 (2002) 500–515.
[58] K.B. Vu, M.A. Ghahroudi, L. Wyns, S. Muyldermans, Comparison of llama VH sequences from conventional and heavy chain antibodies, Mol. Immunol. 34 (1997) 1121–1131.
[59] C. Vincke, R. Loris, D. Saerens, S. Martinez-Rodriguez, S. Muyldermans, K. Conrath, General strategy to humanize a camelid single-domain antibody and identification of a universal humanized nanobody scaffold, J. Biol. Chem. 284 (2009) 3273–3284.
[60] C.R. Anderson, J.J. Rychak, M. Backer, J. Backer, K. Ley, A.L. Klibanov, scVEGF microbubble ultrasound contrast agents: a novel probe for ultrasound molecular imaging of tumor angiogenesis, Invest. Radiol. 45 (2010) 579–585.
[61] B. Geers, I. Lentacker, N.N. Sanders, J. Demeester, S. Meairs, S.C. De Smedt, Self-assembled liposome-loaded microbubbles: The missing link for safe and efficient ultrasound triggered drug-delivery, J. Control. Release 152 (2011) 249–256.
[62] B. Van de Broek, N. Devoogdt, A. D'Hollander, H.L. Gijs, K. Jans, L. Lagae, S. Muyldermans, G. Maes, G. Borghs, Specific cell targeting with nanobody conjugated branched gold nanoparticles for photothermal therapy, ACS Nano 5 (2011) 4319–4328.